INDUSTRIAL PVD METALLIZATION FOR HIGH EFFICIENCY CRYSTALLINE SILICON SOLAR CELLS

Jan Nekarda[1], Dirk Reinwand[1], Andreas Grohe[1], Philip Hartmann[1], Ralf Preu[1], Roland Trassl[2], Stephan Wieder[2]
[1]Fraunhofer Institute for Solar Energy Systems (ISE), Heidenhofstrasse 2, D-79110 Freiburg, Germany
[2]Applied Materials GmbH & Co. KG, Siemensstrasse 100, D-63755 Alzenau, Germany

ABSTRACT

In this paper we present first results concerning different thermal evaporation processes for thin aluminum layers, which are carried out on a pilot system with a throughput of up to 540 wafers/h (156x156 mm²).
To qualify the processes the deposited aluminum layers were evaluated with respect to homogeneity and conductivity. Additionally the effect of the different processes on the passivation quality of a thermally grown 100 nm thick SiO_2 was analyzed by means of lifetime measurements, indicating a negligible effect of the conducted process variations on the passivation quality.
Finally high-efficiency silicon solar cells were prepared to determine the overall potential and to compare it with an electron beam (e-gun) evaporation process, which is used as a standard process in our laboratory. An efficiency of up to 21% was achieved by the high deposition rate technique performing at least as well as our standard high efficiency process.

INTRODUCTION

Promising future technologies like LFC (Laser Fired Contact) or back contacted solar cells require a thin layer of evaporated aluminum as back side metallization [1] . The ATON 500 based system, shown in Figure 1, is to our knowledge the first inline pilot machine capable of such a process in combination with an industrial suitable throughput.
This throughput is achieved by an inline process with thermal evaporation technique, which induces less damage to the passivation than coating by electron beam [2]. Aluminum wires are driven on several heated crucibles, resulting in a continuous generation of aluminum vapor, which condensates on the samples. The wire feed rate as well as the power can be adjusted separately for each crucible to control the homogeneity over the complete tray width as well as the overall deposition rate. The thickness of the aluminum layer can additionally be adjusted by the transport speed of the tray through the machine. Each tray contains nine 156x156 mm² wafers.

Figure 1: Picture of the ATON 500 based evaporation equipment.

BASIC PROCESS SETUP

The thickness of the aluminum layer has a mayor influence on the lateral conductivity and therefore on the efficiency potential of the solar cell.

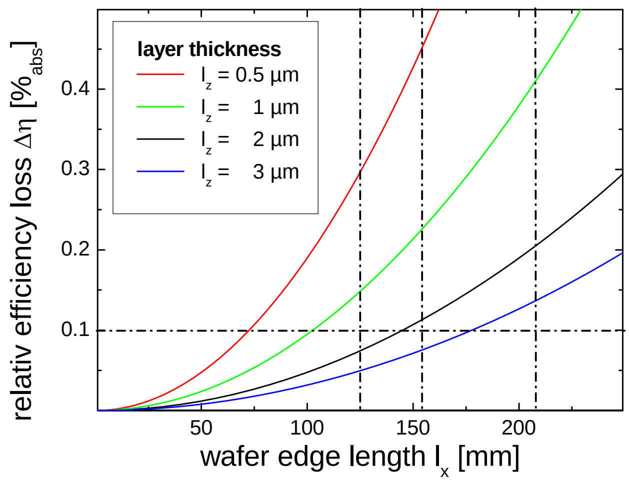

Figure 2: Exemplary efficiency loss shown for different wafer edge sizes when varying the aluminium layer thickness. Assumptions used for the calculations can be found in [3].

Figure 2 shows a simulation of the relative efficiency loss due to the series resistance contribution from a thin rear side aluminum layer which solely contributes to lateral conductance. This rear side structure consisting of a conducting over an isolating layer can be found for example in LFC cells.
Resulting from this calculations (basic assumptions [3]: cell efficiency $\eta = 18\ \%$, maximum power point voltage and current $V_{mpp} = 560$ mV, $J_{mpp} = 35$ mA/cm², two 2 mm wide busbars) the minimum aluminum layer thickness is 2 µm in order to avoid a significant efficiency loss due to an increased sheet resistance and therefore series resistance. The resulting deposition parameters for a first process are listed in Table 1
We investigated a variation in layer thickness using a given deposition rate and varying tray velocities. This results in four different processes (# 2, 4, 5 and 6) leading to layer-thicknesses of 1, 2, 3 and 4 µm. The targeted 2 µm layer thickness was additionally evaluated using three different deposition rates by adjusting the wire feed rate and tray velocities (# 1 – 3).

Table 1: Targeted thickness, tray transport speed and deposition rate of the evaluated processes.

	process	thickness	tray speed	dynamic depos. rate
		[µm]	[m/min]	[µm*m/min]
rate	1	2	0,375	0,75
	2	2	0,75	1,5
	3	2	1,5	3
thickness	4	1	1,5	1,5
	2	2	0,75	1,5
	5	3	0,5	1,5
	6	4	0,375	1,5

Pre-tests show a linear relation between layer thickness and the inverse tray velocity at a constant deposition rate, which allows a simple adjustment of the desired layer thickness using the first approach for parameters 2, 4, 5 and 6. Furthermore, there is a linear behavior between deposition rate and wire feed rate (see Figure 3).

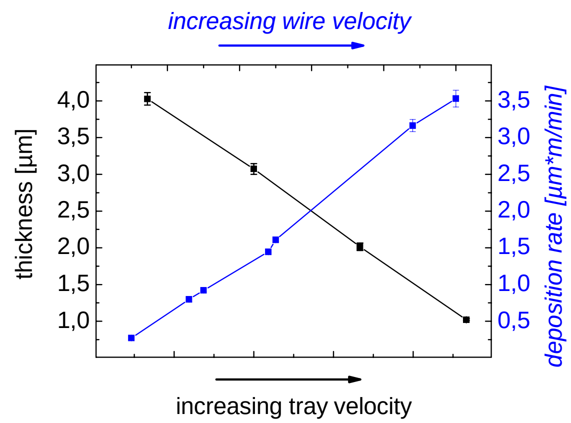

Figure 3: Dependency of layer thickness from tray velocity (deposition rate constant, black) and of deposition rate from wire feed rate (blue).

CHARACTERIZATION OF THE ALUMIUM LAYER

In a first step the homogeneity of the deposited layer was determined by measuring the sheet resistance at 8 x 8 spots on each of the nine 156x156 mm² sized wafers of one tray, which gives a detailed scan over the whole deposition width. The measurements were performed by a four point measurement tool, which allows an excellent spatial resolution. The result on one of the wafer can be seen exemplarily in Figure 4.

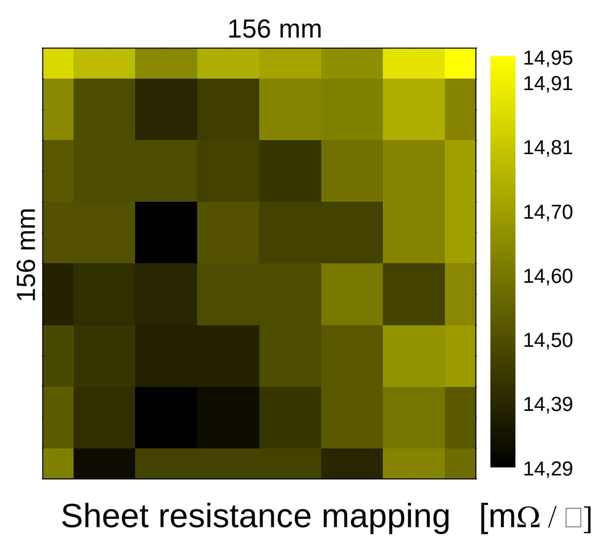

Figure 4: Exemplary sheet resistance measurement of one 156x156 mm² wafer evaporated with 2 µm aluminum during process 1.

The standard deviation σ from the average value is lower than 1.5 % over all 576 points spread out over the tray area, which is insignificant in respect to the following production processes.
The thickness of the deposited layer is measured by two different methods. On the one hand we cooled down 10x10 mm² big evaporated glass samples with nitrogen, broke an edge and analyzed it with a scanning electron microscope (SEM).
On the other hand we covered parts of the sample during the deposition process, which resulted in a sharp edge of the metal layer which can be analyzed by a surface profilometer. Both ways lead to very similar values. Additionally the local sheet resistance was measured on these samples by four point measurements in order to determine the specific resistance of the layer. The results are listed in Table 2. In general the sheet resistance is roughly 1,2 x higher than the literature value for bulk aluminum. Process 2, 3 and 6 lead to a specific resistance of ~3,2 x 10^{-8} Ω*m. Probably due to the smaller deposition rate process 1 results in a slightly lower value of 2,9 x 10^{-8} Ω*m. Obviously there is no strong dependence of the measured sheet resistance from the deposition parameters.

Table 2: Thickness d (profilometer black, SEM blue), sheet resistance R_{sh} and resulting specific resistance ρ_{sh} for different processes.

proc.	d		R_{sh}	ρ_{sh}	
	Ø	σ		Ø	σ
	[µm]	[µm]	[mΩ/sq]	[nΩ*m]	[nΩ*m]
1	1,83	0,042	15,86	29,0	0,7
1	1,87	0,071	15,38	28,8	1,1
2	2,11	0,021	15,37	32,4	0,3
2	1,98	0,007	16,02	31,6	0,1
3	1,97	0,028	16,42	31,0	2,4
3	*2,10*		*15,73*	*33,0*	
6	4,23	0,141	7,72	32,3	1,1
6	4,19	0,092	7,66	32,3	0,7

CHARACTERISATION REGARDING SOLAR CELL REAR SIDE METALLIZATION

Beside a well assessable homogeneity and layer thickness a metallization process used in solar cell production should maximize the internal reflection and must not deteriorate the subjacent passivation. Therefore the influence of the deposition process on the passivation quality was evaluated by measuring the minority carrier lifetime in silicon using symmetrical samples consisting of 1 Ω*cm FZ wafers with 100 nm thermally grown SiO_2. The process flow of these structures is shown in Figure 5.

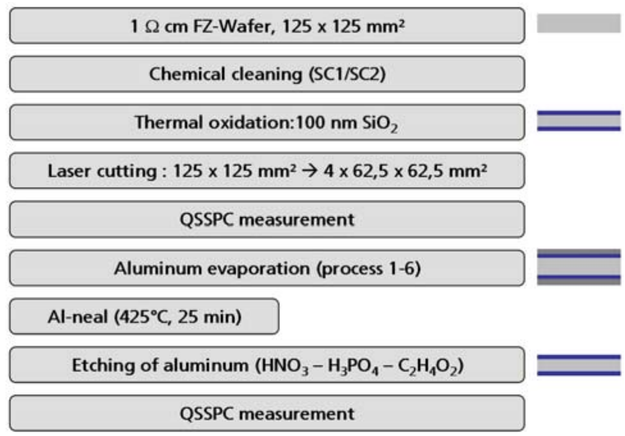

Figure 5: Process flow (left) and schematic appearance (right) of the “lifetime samples”.

The carrier lifetime was measured after oxidation using the Quasi Stady State Photoconductance technique (QSSPC) [4]. Afterwards aluminum was evaporated on both sides of 4 samples during each of the different processes 1-6. Since the lifetime can be enhanced by a following low temperature process (Al-neal), one half of the samples were annealed at 425°C for 25 minutes under forming gas. Afterwards the aluminum was removed from all samples using an HNO_3 – H_3PO_4 – $C_2H_4O_2$ solution and measured by QSSPC again. The results can be seen in Figure 6.

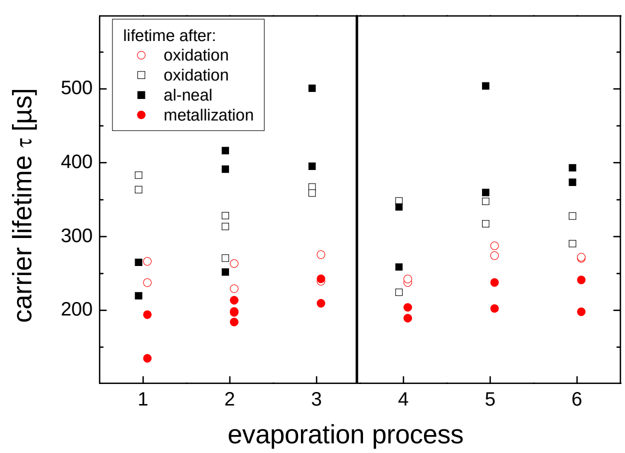

Figure 6: Results of QSSPC lifetime measurements before metallization (open symbols) and after the different deposition processes 1-6 with (black) and without (red) a following low temperature process (al-neal).

Lifetimes after thermal oxidation range around 250 – 400 µs. After evaporation the lifetimes drop to about 150 – 250 µs for all processes. The additional Al-neal process leads to higher carrier lifetimes than before metallization except for the deposition processes 1 (small evaporation rate) and 4 (thinner layer of 1 µm). Despite the variation between the single samples it is obviously that the induced damage to the passivation layer can be overcompensated by a post-metallization anneal for most deposition processes, resulting in lifetimes of over 500 µs. The reason for the reduced positive impact of the Al-neal process on the lifetime level of processes 1 and 4 is not yet understood and needs further investigation.

One possible parameter which can influence the quality of the passivation layer is the deposition temperature. Therefore the temperature of process 2, 4 and 5 was recorded using thermocouples spread over three as-cut wafers distributed over the complete tray width and the temperature measurement console “super M.O.L.E. Gold” from ECD [5].

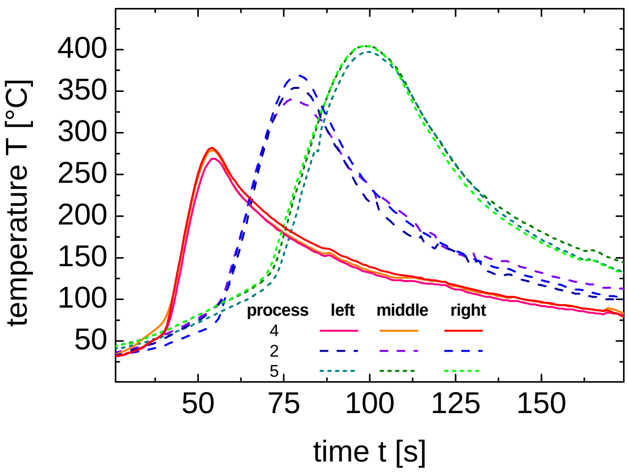

Figure 7: Wafer temperature during processes 2 (blue), 4 (red) and 5 (green) on the right, in the middle and on the left side of the tray.

The results of the measurements are shown in Figure 7. The temperature is constant over the width of the tray and rises rapidly to the peak before dropping with an exponential decay. Although the peak temperature rises with increasing layer thickness and reaches values of 270 °C (1 µm Al), 370 °C (2 µm Al) and 400 °C (3 µm Al), all processes lead to similar lifetime values.

Due to the increased impact of the internal reflection on thin solar cells we compared the values in respect to the different deposition processes. Within a solar cell batch which is described more closely in the next section, the influence of the different evaporation processes could be evaluated. All of the aluminum layers were deposited on 100 nm thermal oxide.

Figure 8 shows that the difference in internal reflection on the back side (λ > 1000 nm) between the different processes themselves as well as when being compared with the e-gun reference is very small. The variation results most probably from different external reflection of the measurement beam on the front side grid.

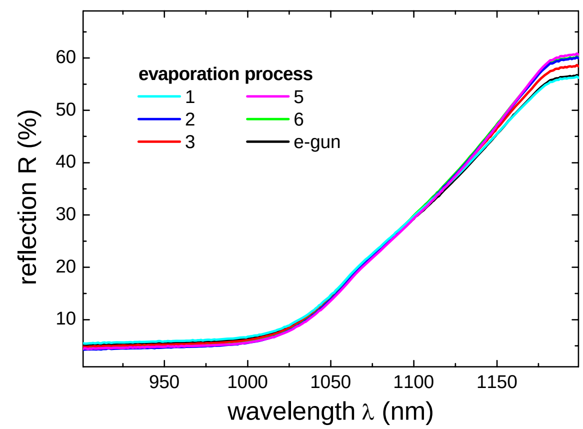

Figure 8: Reflection of high efficiency solar cells with 100 nm thermal oxide passivation and different evaporation processes

FABRICATION OF HIGHLY EFFICIENT SOLAR CELLS

To evaluate the overall potential of the investigated processes high efficient solar cells were manufactured as shown in Figure 9.

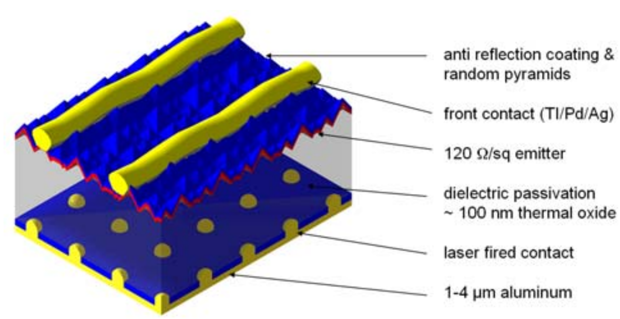

Figure 9: Schematic structure of the high efficient solar cell used for determining the potential of different evaporation processes.

Seven 20x20 mm² cells are distributed on a p-type 1 Ohm*cm float zone wafer. The cells feature a phosphorous emitter with a sheet resistance of 120 Ohm/sq on a random pyramid textured surface and a 100 nm thick

thermally grown SiO_2 front and rear side passivation. The front contact grid is defined by photo lithography, evaporation of a thin TiPdAg layer, lift-off and subsequent electroplating in silver. For the rear side we used the evaluated thermal evaporation process 1-6. Reference cells have been coated using a lab type e-gun evaporation system with planetary rotation of the wafers during processing. The rear contacts are formed by laser firing (LFC). Afterwards all cells underwent an identical Al-nealing process as the lifetime samples (425°C, 25 min., forming gas).
Due to front side metallization problems only few cells reached the expected efficiency and therefore a comprehensive comparison of the different processes is not possible. Nevertheless, the best cell overall was metalized with process 1 and reached an efficiency of 21 %. This already indicates the potential of the evaluated evaporation processes.

Table 3: Cell parameters of the best solar cells with rear side aluminum evaporation by process 1 as well as by the laboratory e-gun system

PVD method	V_{OC}	J_{SC}	FF	η
	[mV]	[mA/cm²]		[%]
e-gun	668,4	39,03	0,794	20,7
high rate thermal	665,0	39,14	0,805	21,0

Besides a slightly higher open circuit voltage, the cell parameter of the best cell evaporated with the laboratory e-gun system reveals no major difference as can be seen in Table 3

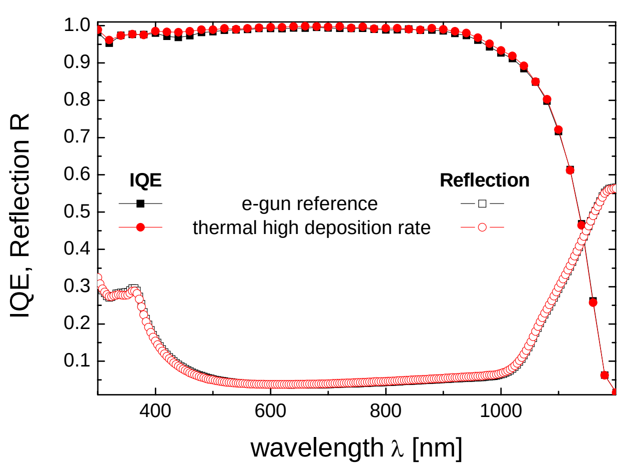

Figure 10: Comparison of the Internal Quantum Efficiency (IQE) and reflection of the best solar cells of process 1 and e-gun reference process.

When comparing the internal quantum efficiencies (IQE, see Figure 10) again no major differences can be seen.

SUMMARY

Several different thermal evaporation processes have been investigated. Generally the evaluated equipment is able to deposit aluminum layer of different thicknesses with nearly ideal sheet resistance and homogeneity.
These processes in combination with thermal oxide lead to comparable values of the internal reflection and very good carrier lifetimes of up to 250 µs after deposition, which still can be increased to values > 500 µs with a subsequent al-neal process.
Compared to a standard electron beam evaporation process, similar cell efficiencies of up to 21 % are reached. These results in combination with the throughput of 540 cells per hour (156x156 mm²) already indicate the applicability of this pilot system for the industrial metallization of future solar cells.

ACKNOWLEDGEMENTS

The authors would like to thank S. Seitz for sample preparation, E. Schäffer for cell measurements and Robert Zacharias for temperature measurement.
The financial funding by the “Bundesministerium für Umwelt, Naturschutz und Reaktorsicherheit” (german ministry for environment, nature conservation and reactor safety) under the contract no. 0325025B is greatly appreciated.

REFERENCES

1. Schneiderlöchner, E., et al., *Laser-fired rear contacts for crystalline silicon solar cells.* Progress in Photovoltaics: Research and Applications, 2002. 10: p. 29-34.
2. Grohe, A., et al. *Boundary conditions of the industrial production of LFC cells*. in *Proceedings of the 4th World Conference on Photovoltaic Energy Conversion*. 2006. Waikoloa, Hawaii, USA.
3. Grohe, A., *Einsatz von Laserverfahren zur Prozessierung von kristallinen Silizium-Solarzellen*, in *Fakultät für Physik*. 2007, Universität Konstanz: Konstanz.
4. Sinton, R.A., A. Cuevas, and M. Stuckings. *Quasi-steady-state photoconductance, a new method for solar cell material and device characterization*. in *Proceedings of the 25th IEEE Photovoltaic Specialists Conference*. 1996. Washington DC, USA: IEEE; New York, NY, USA.
5. Datasheet "Super M.O.L.E. gold", www.ECD.com